ELSEVIER

Ceramics International 33 (2007) 605–614

CERAMICS INTERNATIONAL

www.elsevier.com/locate/ceramint

Electrochemical and structural characterisation of zirconia reinforced hydroxyapatite bioceramic sol–gel coatings on surgical grade 316L SS for biomedical applications

A. Balamurugan [a,*], G. Balossier [a], S. Kannan [b], J. Michel [a], J. Faure [a], S. Rajeswari [b]

[a] *INSERM ERM 0203, Laboratoire de Microscopie Electronique Analytique, Université de Reims, 21, Rue Clément Ader, 51685 Reims, France*
[b] *Department of Analytical Chemistry, University of Madras, Guindy Campus, Chennai 600 025, India*

Received 21 June 2005; received in revised form 25 October 2005; accepted 14 November 2005
Available online 20 February 2006

Abstract

Yttria-stabilized zirconia (YSZ)/hydroxyapatite (HAP) composite coatings on surgical grade 316L stainless steel was carried out using sol–gel dip coating and calcination process. Various molar ratios of HAP and YSZ was developed, each YSZ/HAP gel coating showed an average particle size of ~30 nm and the coatings were dried and calcined for crystallization. The functional group and crystallization characteristics of the coatings were analyzed using (FT-IR), X-ray diffraction (XRD) and energy dispersion X-ray analysis (EDXA). The formation of β-tricalcium phosphate (β-TCP) was controlled changing the Ca/P ratio in HAP phase and also YSZ content in the composite coatings. It was revealed that TCP content showed a very minimum value at Ca/P ratio of ~1.67 and at YSZ content of 30 vol.%, respectively. The mechanism of increased β-TCP content with Ca/P ratio lower than 1.67 and increased YSZ content was explained as Ca-deficiency due to the Ca-diffusion into t-ZrO_2 crystals to form a solid solution. The resultant coatings were analysed for its corrosion resistance through polarisation, impedance and ICP-AES analysis in simulated body fluid. The viability of the reinforced coatings were analysed by in vitro cell culture studies.

Keywords: C. Corrosion; Sol gel; Zirconia; Hydroxyapatite; Reinforcement

1. Introduction

Calcium phosphate compounds have been studied for biomedical applications due to their analogy to the inorganic component of natural bones and teeth [1]. With Ca/P ratio calcium phosphate ceramics form different stable phases including hydroxyapatite ($Ca_{10}(PO_4)_6(OH)_2$:HAP) and other phases such as tricalcium phosphate ($Ca_3(PO_4)_2$:TCP) and tetracalcium phosphate ($Ca_4(PO_4)_2O$:TTCP) [2]. It has been well known that HAP is bioactive and biocompatible with human tissues, while the others are highly bioresorbable [3]. However, bioceramic coatings containing HAP alone is not suitable for most of artificial hard tissue applications due to their high brittleness and low wear resistance. Thus, to improve the mechanical properties of HAP materials the reinforcement of ZrO_2 has been attempted. The reinforcing phase in the form of ZrO_2 particles was selected due to the satisfactory biocompatibility of ZrO_2 and also because of its exceptional mechanical properties. However, the addition of ZrO_2 causes an increase in the content of β-TCP which is a bioresorbable phase. Some amount of β-TCP in HAP would be helpful for the rapid bonding of artificial bones to natural ones via rapid dissolution [4,5]. However, too a high content of β-TCP seriously deteriorates the mechanical properties and chemical stability of artificial bones. Thus, the precise control of β-TCP content in HAP is a critical issue in biomedical applications. In this study, yttria-stabilized (Y_2O_3) tetragonal zirconia was used to form YSZ/HAP composite and a sol–gel route was employed for the development of coatings. The Ca/P ratio and YSZ content in the YSZ/HAP composite were changed to control β-TCP phase formation. The β-TCP content variation was identified using X-ray diffraction (XRD) analysis. The obtained coatings were subjected to the electrochemical, structural and mechanical analysis to study their stability. Furthermore, in order to evaluate the cell viability, the osteoblastic cellular responses to the reinforced composite coatings were assessed.

* Corresponding author. Fax: +33 3 26 05 75 64.
E-mail address: abmurugan@yahoo.co.in (A. Balamurugan).

0272-8842/$32.00
doi:10.1016/j.ceramint.2005.11.011

2. Materials and methods

2.1. Sample preparation

Zirconium isopropoxide $Zr(OC_3H_7)_4$ diluted in isopropanol was used as the source of zirconia. Yttrium acetate and glacial acetic acid were used as stabilizing agents. The source solution was homogenized with stabilizing agents under ultra sound irradiation condition at 20 kHz. To obtain monophasic HAP, triethyl phosphite and calcium nitrate precursors were prepared by dissolving in anhydrous ethanol. Both calcium and phosphorus precursors were mixed together to obtain a stoichiometric Ca/P ratio and this solution was finally added to the sol of ZrO_2. The reinforcements were prepared by varying ZrO_2 sol concentration from 10 to 50 vol.% and the concentration of calcium and phosphorus solution was kept constant to keep the stoichiometry of HAP(∼1.67). The reinforcement solutions were constantly stirred for 17 h followed by 36 h of ageing. After ageing the solutions were moved into the coating bath for dip coating of the stainless steel specimens. The obtained coatings were dried at 40 °C and calcined at various temperatures to get adherent crystalline coating. The schematics for the development of coatings is shown in Fig. 1.

2.2. Characterisation of the coatings

The functional characteristics of reinforced coatings (ZrO_2/HAP) were analysed with FT-IR (Perkin-Elmer FT-IR Paragan series instrument). The spectra were recorded from 4000 to 400 cm^{-1} wave number with a resolution of 4 cm^{-1}. The thermal behavior of the coatings were performed through thermo gravimetric analysis (TGA) and differential thermal analysis (DTA) using a (Seiko Instruments Inc, Japan). Twenty to twenty-five milligrams of the sample was taken in platinum crucible in the temperature range from 20 to 1500 °C at a heating rate of 10 °C/min in air atmosphere. DTA was performed along with TGA, which enables the change in weight to be correlated with the reactions observed from the exothermic peak. The thickness of the coatings were measured by using the sensing probe of ELCA-D meter (Germany). The specimens obtained at the optimum coating conditions were subjected to heat treatment at various temperatures in an Indotherm 401 air furnace at a heating rate of 10 °C/min for an hour. The samples were removed after cooling in the furnace and were stored in vacuum desicator and analysed by XRD for phase morphology. All the ceramic-coated 316L SS were subjected to SEM-EDXA analysis for the chemical constituent changes that have occurred on the surface and the observation of microstructure. The instrument Philips 501 scanning electron microscope (SEM) equipped for X-ray microanalysis was used for the microstructural and microanalysis. The samples were coated with a thin layer of gold using an Edwards sputter coater S150B instrument. The shear bond strength analysis of all the reinforced coated 316L SS were performed as per ASTM international standard D 4501 and F1044. 316L SS steel strips (10 mm × 50 mm × 2 mm size) were used for the analysis. For specimen preparation, the strips were polished and dip coated with ceramics (ZrO_2/HAP). The coupling strip was also polished, glued (epoxy resin) with thermoplastic and then joined under pressure in a fixture to the strip with ceramic coatings. The couples, cured at 98 °C for 1 h were subjected to the shear test. A universal testing machine (Model 5569, Instron, Canton, MA) was used to determine the shear bond

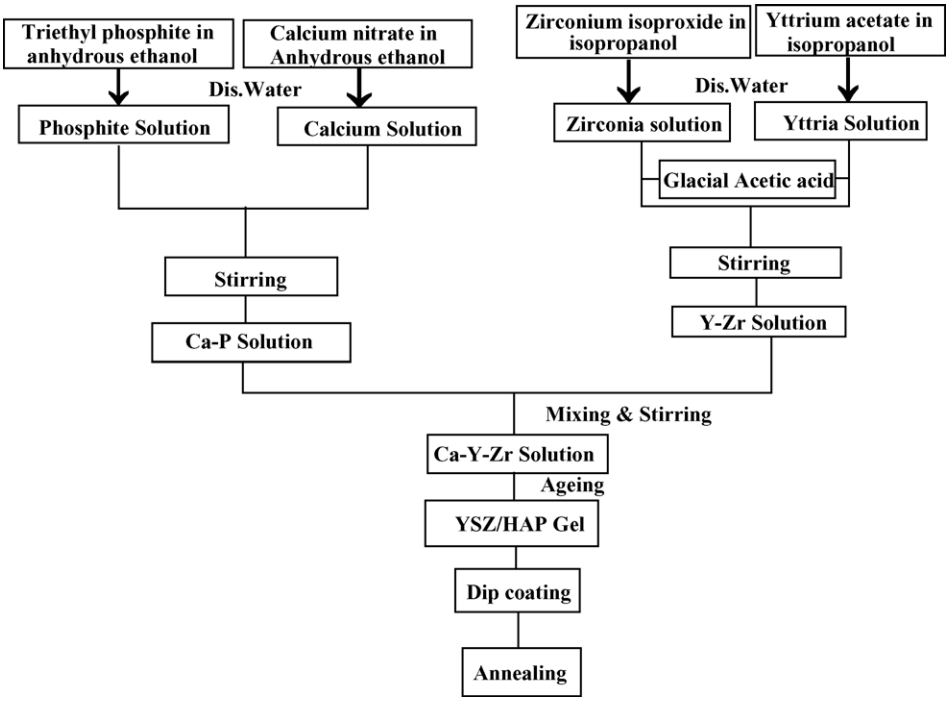

Fig. 1. Schematic representation of ZrO_2 reinforced HAP coating.

strength of the coatings. The maximum speed at full load was 250 mm/min for each testing material and five samples were tested for every coating and the data are reported as the average value.

2.3. In vitro cell culture analysis

Osteoblasts were isolated by sequential trypsin–collagenase digestion on calvaria of neonatal (<2 days old) Sprague–Dawley rats as described elsewhere [6]. In this study, only the cells at the 2nd to 5th passage were employed. For evaluation of osteoblasts adhesion, the cells were seeded on each disc at a density of 8000 cells/cm^2. After culturing for 6 and 24 h, the discs were dyed with Giemsa solution, and observed by optical microscopy (Leica S6D, Germany). For SEM observation, the discs were dehydrated in a grade ethanol series (30, 50, 70, 90 and 96% (v/v)) for 10 min, respectively, with final dehydration in absolute ethanol twice followed by drying in hexamethyldisilizane (HMDS) ethanol solution series [7]. For evaluation of osteoblasts proliferation, the cells were seeded at a density of 3500 cells/cm^2. After culturing for 1, 3 and 5 days, the discs were dyed with Giemsa solution, and counted under optical microscopy. Cell density (cells/cm^2) was determined by averaging the number of adherent cells in six randomly selected fields per substrate.

2.4. In vitro electrochemical analysis

In this study, the open circuit potential (OCP)–time measurements, cyclic polarization experiments, impedance measurements and ICP-AES were used as the criterion for the evaluation of sol–gel reinforced coatings on surgical grade 316L SS (Table 1). The localized corrosion behaviors of the samples were studied in simulated body fluid Ringer's solution (Table 2). The cell assembly and the electrode preparation for in vitro electrochemical studies are as detailed else where in Ref. [8]. The temperature of the polarization cell was maintained at 37 ± 1 °C by means of a thermostat water bath to simulate the human body temperature. Before immersing the specimen into the electrolyte, purging of solution was done by using purified nitrogen in order to remove dissolved gases such as oxygen, CO_2, etc., and purging was maintained throughout the experiment. The corrosion measurements were carried out as per ASTM standards. The electrochemical impedance tests were carried out in BAS system (Germany) and the data were plotted and analyzed using Z view software version 1.5b, (C) 1996, Scribner Associates Inc. The leaching of the metal ions can be accelerated under in vitro conditions by impressing a suitable potential for a specified duration of time. This method is a simulation of long-term contact of metallic implants with biological system, which can be achieved, in short duration of time. In this leaching method, the coated materials are kept at a constant potential in the passive region. In the present study, impressed potentials of (200, 300, 400, and E_b) were applied on the pristine and ceramic-coated specimens for 60 min in 200 ml of Ringer's solution. At the end of each experiment the leaching of metal ions in the test solution was analysed by Inductively Coupled Plasma Atomic Emission Spectroscopy (Thermo Jerral Ash-Atom Scan, USA).

Table 1
Composition of surgical grade 316L SS

	Alloy								
	C	Mn	Cr	Ni	Si	Mo	P	S	Fe
316L SS	0.029	1.8	17.3	12.4	0.7	2.25	0.031	0.012	Bal

Table 2
Chemical composition of Ringer's solution

Solution	Chemical reagent	Weight (g/l)
Ringer's solution	NaCl	8.60
	$CaCl_2{\cdot}2H_20$	0.66
	KCl	0.60

3. Results and discussions

3.1. Characterisation of the coatings

It is always desirable that HAP coating stays on the surface of an implant in a biological environment as long as possible. However, the bond strength of HAP coating/metal substrate interface has been the point of potential weakness in prosthesis because it is limited by the strength of hydroxyapatite, porosity, and inclusion in the lamellar structure of the coating. Recent research has shown that the mechanical properties of HAP coatings can be improved by the reinforcement of yttria-stabilised zirconia [9]. In vitro test results indicate that the dissolution rate of HAP/zirconia composite coatings is slower than that of HAP coatings; bond strength and the corrosion resistance of HAP/zirconia coatings are superior to that of HAP coatings. In the present investigation 10, 30 and 50 vol.% of zirconia, respectively, have been added to the HAP sol to improve the properties of the coatings (nomenclature given as HAP + Z10, HAP + Z30 and HAP + Z50). The effects of zirconia on the phase composition, microstructure, bond strength and corrosion resistance of the HAP/zirconia reinforced coatings have been evaluated.

3.1.1. Effect of sintering

High-temperature sintering processes have been used to produce reinforced ZrO_2/HAP composite coatings. In the earlier reports, the temperature used during the sintering process often was as high as 1400 °C [10]. This processing temperature is considered insufficient regarding the sintering and densification of zirconia, but very high while considering the decomposition of hydroxyapatite. The initial phase composition in the ZrO_2/HAP reinforced material was reported to be changed during the sintering, according to the following reaction:

$$Ca_{10}(PO_4)_6(OH)_2 \rightarrow 3Ca_3(PO_4)_2 + CaO + H_2O \quad (1)$$

After decomposition, the CaO was dissolved into the zirconia matrix. The additional amount of CaO produced a

phase change from tetragonal to cubic, and in some cases, calcium zirconate also formed. In samples where severe decomposition of the HAP occurred, tricalcium phosphate was the only decomposed product found. Therefore, it was proposed that the decomposition of HAP was related to the transfer of CaO to the zirconia matrix. As a result of this loss of CaO, the decomposition of HAP resulted in the formation of tricalcium phosphate [11,12]. The reaction that occurs between zirconia and HAP may influence both strength and the biological properties of sintered materials [13]. To a large extent, the mechanical strength of zirconia depends on the phase transformation from the tetragonal phase to the monoclinic phase. A complex problem observed in the ZrO_2/HAP system is related to the phase changes and decomposition reactions. Hence, the optimization of the annealing temperature is necessitated.

With increasing temperature, the loss of water from the HAP is initiated at ~600 °C and an oxyhydroxyapatite is formed. At a temperature range of 1000 °C, a sufficient fraction of OH^- ions are lost from the oxyhydroxyapatite. The reaction course may continue with decomposition of the apatite phase, when the zirconia reacts with oxyhydroxyapatite instead of HAP.

Based on the XRD results of the sol–gel reinforced coatings with 30 vol.% of zirconia reinforced HAP, stoichiometry of the HAP was found stable up to the annealing temperature of 950 °C. Sintering above this particular temperature caused the decomposition of HAP to tricalcium phosphate at the range of 1050 °C. The amount of TCP formed increased with increasing sintering temperature, and HAP was decomposed completely at a temperature of 1400 °C, according to the XRD patterns. The decomposition reaction is divided into two steps:

$$Ca_{10}(PO_4)_6(OH)_2 \rightarrow Ca_{10}(PO_4)_6(OH)_{2-2x}O_x + xH_2O \quad (2)$$

$$3Ca_{10}(PO_4)_6(OH)_{2-2x}O_x + yZrO_2(t) \rightarrow 3Ca_3(PO_4)_2 + CaO[ZrO_2(c)]y + (1-x)H_2O \quad (3)$$

However, if the water loss is maintained at a low level, the equilibrium in the first reaction is shifted to the left and the second reaction may not occur. Thus based on the results, the sintering temperature for ZrO_2/HAP reinforced coating was chosen as 950 °C.

3.1.2. IR spectroscopy

Fig. 2a and b are representatives of the FT-IR spectra of the HAP reinforced zirconia coatings (HAP + Z50, HAP + Z30), respectively. The spectra recorded low intensity absorption bands of P–O due to PO_4^{3-} groups in the 1080–1020 cm^{-1} region, which are characteristic of HAP as well as of the O–H–O bands of absorbed water. A small shoulder associated with the O–H vibrational mode around 600–610 cm^{-1} is seen in the HAP + Z50 coating but is absent in the HAP + Z30 coating. Bands or shoulders of O–H stretching at 3600–3580 cm^{-1} and of the ZrO_2 phase were not identified for these coatings, although CaO absorption bands at 250–200 cm^{-1} were found in their spectra. The effect of ZrO_2 on the OH^- ions associated with the stretching mode at 3600–3580 cm^{-1} tends to intensify this absorption band in the IR spectra. The IR spectra for both

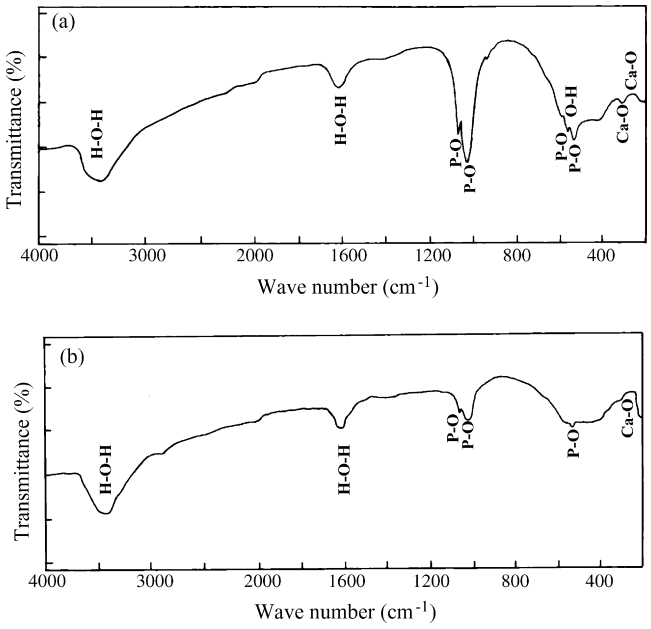

Fig. 2. FT-IR spectra of ZrO_2 reinforced HAP coatings on 316L SS (a) HAP + Z50; (b) HAP + Z30.

the samples studied do not show absorption bands corresponding to ZrO_2. This is due to the disappearance or masking of the O–H stretching mode, caused by the coexistence of CaO–Zr–O and ZrO_2, as reported in the XRD patterns. Thus, the simultaneous analysis of XRD and FT-IR spectra indicates that the content of zirconia phase in HAP + Z30 reinforcement have shown a great impact on the structural features of HAP phase [14].

Based on the spectral data, which indicates Zr^{4+} ion substitutions in the apatite crystal structure, a hypothetical substitution mechanism is proposed. This involves the replacement of two calcium ions of HAP phase by one zirconium ion ($2Ca^{2+} = Zr^{4+}$). The substitution reaction $2Ca^{2+} = Zr^{4+}$ may be represented as:

$$Ca_{10}(PO_4)_6(OH)_2 + nZr^{4+}[HAP] = Zr_nCa_{(10-2n)}(PO_4)_6(OH)_2 + 2nCa^{2+}$$

The probable incorporation of Zr^{4+} ion into the HAP phase lattice, resulting in a Zr-for-Ca substitution, may be a consequence of its smaller ionic radius in comparison to that of Ca^{2+} ion.

3.1.3. X-ray diffraction analysis

The experimental results showed that the addition of ZrO_2 induces the formation of TCP. The coatings with Z30 formed a small amount of TCP Fig. 3. The coatings with the addition of 10, 50 vol.% ZrO_2 consisted of a considerable amount of CaO, i.e., at the same experimental conditions, the more ZrO_2 added the higher the amount of CaO formed [15]. Fig. 4 indicates that the addition of ZrO_2 increases the formation of TTCP and TCP significantly. X-ray patterns showed that $CaZrO_3$ formed with the addition of Z50, whereas there was a trace of $CaZrO_3$ in the reinforced coating containing Z30. This indicates that the

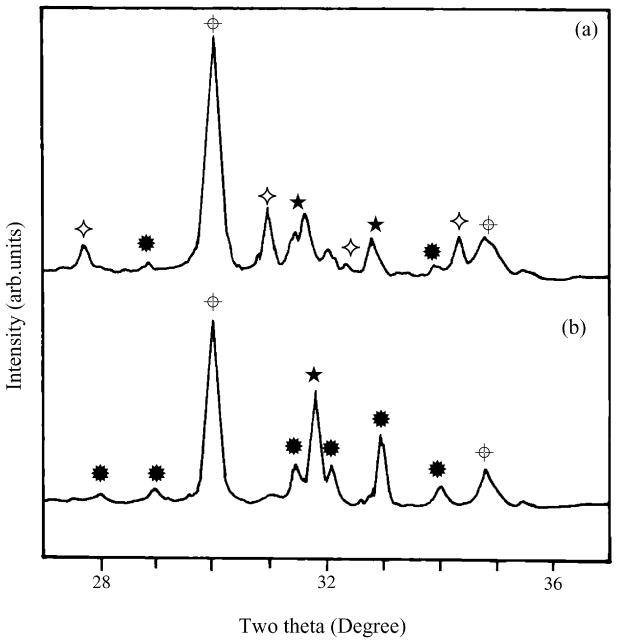

Fig. 3. XRD patterns of (a) HAP-50 vol.% of ZrO_2; (b) HAP-30 vol.% of ZrO_2 reinforced coatings after sintering at 1100 °C. (✹) HAP, (⌖) ZrO_2, (★) $CaZrO_3$ (✧) TCP.

increasing content of zirconia results in the increased formation of $CaZrO_3$ in the coatings. Investigating the bulk ZrO_2/HAP reinforced composite at 1050 °C, found that the CaO in the HAP diffuses into ZrO_2 to cause the tetragonal ZrO_2 transformation into cubic ZrO_2 [11,16]. The loss of CaO will then accelerate the decomposition of HAP into β-TCP at >900 °C. The reaction of the study is as follows.

$$\text{Y-}ZrO_2(t) + Ca_{10}(PO_4)_6(OH)_2 \rightarrow CaO\ \text{Y-}ZrO_2\,(c) + 3\beta\text{-}Ca_3(PO_4)_2 + H_2O \quad (4)$$

It is also found the transformation of tetragonal ZrO_2 into cubic ZrO_2 phase after sintering; however α-TCP was the decomposition product rather than β-TCP [17]. The following reaction occurred simultaneously;

$$Ca_{10}(PO_4)_6(OH)_2 \rightarrow 3\alpha\text{-}Ca_3(PO_4)_2 + CaO + H_2O \quad (5)$$

$$ZrO_2(t) + CaO \rightarrow CaO\text{-}ZrO_2\,(c) \quad (6)$$

Direct reaction between HAP and ZrO_2 was also assumed as:

$$Ca_{10}(PO_4)_6(OH)_2 + ZrO_2 \rightarrow \alpha\text{-}Ca_3(PO_4)_2 + CaZrO_3 + H_2O \quad (7)$$

XRD patterns of the dip coated HAP/YSZ obtained at the sintering temperature of 950 °C is shown in Fig. 4a pattern with Z10 addition, (b) pattern with Z30, (c) Z50 addition. Referring to the XRD patterns, the coating with Z50 consists of ZrO_2, crystalline HAP, amorphous HAP and a trace of TCP. At Z30, the main phases were ZrO_2, crystalline HAP, amorphous HAP phase with a small amount of $Ca_3(PO_4)_2$ (TCP), $Ca_4P_2O_9$ and (TTCP) with a small amount of $CaZrO_3$. Tetragonal zirconia remained stable during sintering and no other zirconia phases appeared after sintering.

Accordingly, more crystalline HAP was transformed to amorphous calcium phosphate. $CaZrO_3$ formation came from the reaction between CaO and ZrO_2 instead of the direct reaction between HAP and ZrO_2. This can be inferred from the XRD results of the coatings with different amounts of zirconia in Fig. 4. If $CaZrO_3$ came from the direct reaction between HAP, ZrO_2, $CaZrO_3$ should be formed more at Z50 and the amount of $CaZrO_3$ in Z50 should be higher than that of Z10. In fact, no $CaZrO_3$ formed with the addition of Z30 and more $CaZrO_3$ appeared in the coatings containing Z10 along with the excess CaO.

3.1.4. Thermal analysis

The TGA and DTA curves of the reinforced coatings are shown in Fig. 5a and b. There are no significant differences in the composite coatings of HAPZ30 and HAPZ50. Weight losses were about 3.5 and 4.5% for HAPZ30 and HAPZ50, respectively, for temperatures from 25 to 1400 °C. A relatively pronounced mass loss occurs between 25 and 100 °C, with the associated endothermic peak attributed to adsorbed water. From 100 °C, a slight decrease in TGA curves corresponding to a loss of about 2.5% is verified up to 900 °C. Another endothermic peak (at 1100 °C) can be attributed to the decomposition of HAP into oxyapatite, which in turn, converts to tricalcium phosphate (TCP) and tetra calcium phosphate (TTCP). After this peak, no other thermal change is observed up to 1400 °C. In other words, thermal stability was achieved for both the reinforced coatings.

3.1.5. EDXA analysis

The energy dispersion X-ray analysis shows the surface chemical composition of ZrO_2/HAP reinforcement coating in Fig. 6.The analysis revealed that calcium and phosphorus is in the desired ratio and no alteration was noticed in the stoichiometric HAP. The spectrum revealed the presence of prominent HAP and Zr crystal phases. Peaks corresponding to

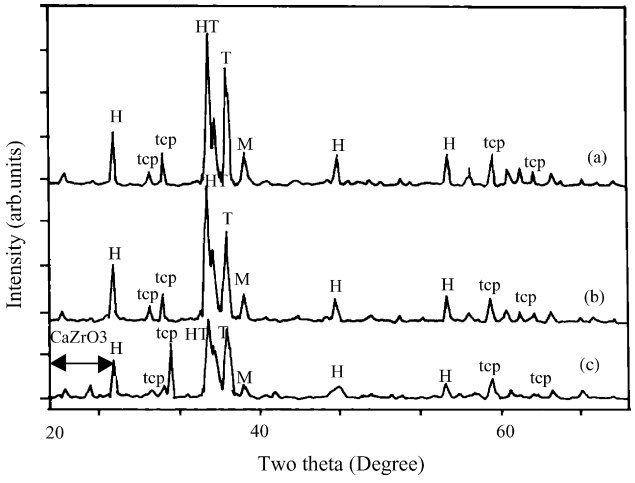

Fig. 4. XRD patterns of HAP + ZrO_2 coatings on 316L SS (a) HAP + Z10; (b) HAP + Z30; (c) HAP + Z50. H, HAP; TCP, tricalcium phosphate; T, tetragonal zirconia; M, monoclinic zirconia.

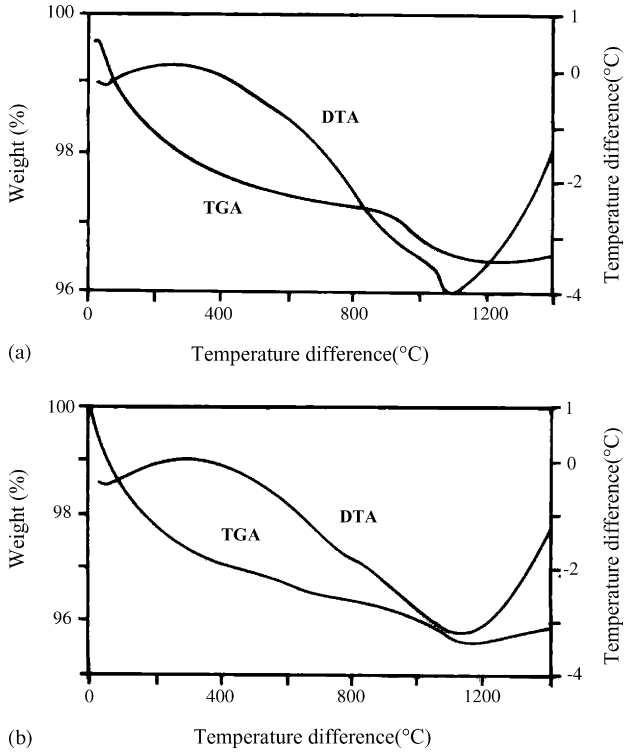

Fig. 5. TGA and DTA curves for (a) HAPZ30 and (b) HAPZ50 coatings on 316L SS.

Fe, Cr and Ni present in the candidate material were also obtained. The studies confirm that the sol–gel ZrO_2/HAP coating and further annealing treatment did not alter the stoichiometry of the hydroxyapatite.

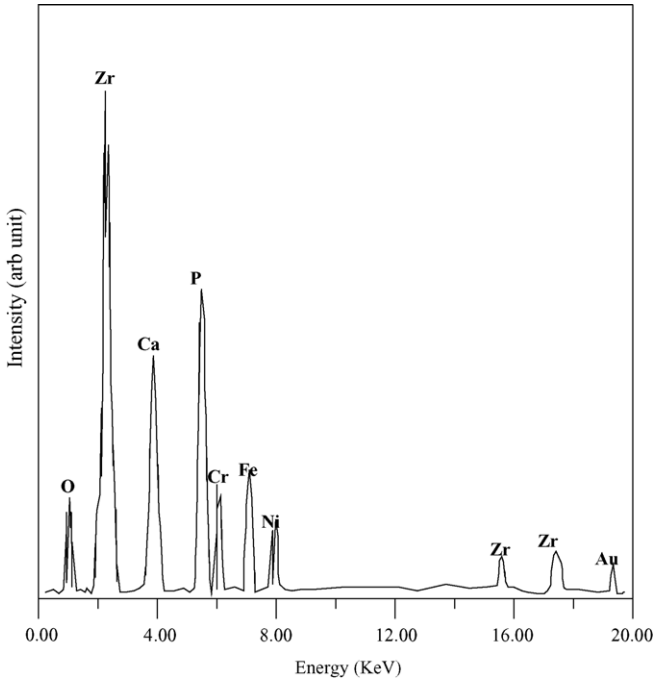

Fig. 6. EDXA spectrum of the reinforcement coating of ZrO_2/HAP on 316L SS.

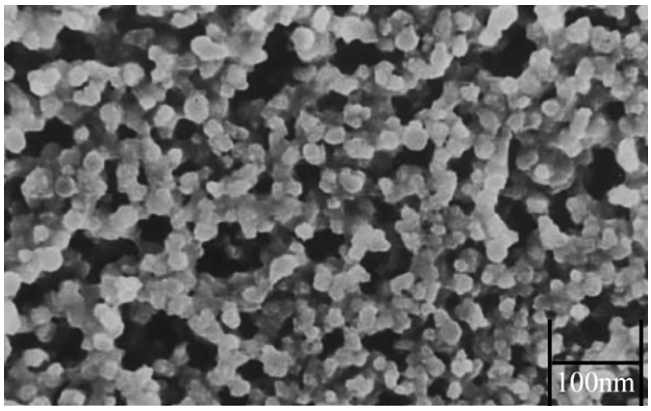

Fig. 7. Micrograph shows the crystalline grain structure of the ZrO_2/HAP on surgical grade 316L SS.

3.1.6. Morphological studies

Fig. 7 shows an SEM image of a zirconia reinforced hydroxyapatite sol–gel coating. The image corresponds to a single layer sintered at 900 °C for 2 h. As can be seen, a very homogeneous crystalline grain structure of about 30 nm has developed, in good agreement with X-ray results. A close inspection of the Fig. 7 reveals additional information about the microstructure of reinforcements. The grains are interconnected, forming groups (usually four-five grains), and apparently, the main porosity seems to be associated with the intergroup regions. However, this intergranular porosity is much less than the measured value (63%), suggesting the existence of internal porosity within the grains, probably at the nanometer scale.

Fig. 8a showed the homogeneous microstructure of the coating with an average grain size of 30 nm for zirconia and 20 nm for HAP. Thus, under the applied sintering conditions the grain growth in zirconia reinforcement ceramics. Fig. 8b progresses more rapidly to form a microstructure of sub-micron size with nearly equiaxed grains and further develops an interlocking elongated fine particles within few minutes. The grain growth rate strongly depends on the nature of the precursor and the applied heating rate. It is thus possible to adjust the microstructures of the produced HAP/ZrO_2 ceramics by manipulating the grain growth kinetics and accordingly to tailor their mechanical properties.

3.1.7. Mechanical properties

At the molecular level, the high adhesion strength values is possible with alkoxide-based sol–gel film systems bonding at the interface between the alkoxide molecules and the free hydroxyl groups at the metal oxide surface. This is essentially a condensation reaction similar to that occurring in alkoxide molecule. However, despite inferences of substrate surface oxide to film oxide bridging, no direct evidence of such bonding was demonstrated and this adhesion mechanism remains speculative (Fig. 9).

Still, an important consideration in this model is the existence of a surface metal oxide, most of which are known to be hydroxylated in the presence of water or water vapour. The reinforced ZrO_2/HAP film deposited with 23 μm thickness was

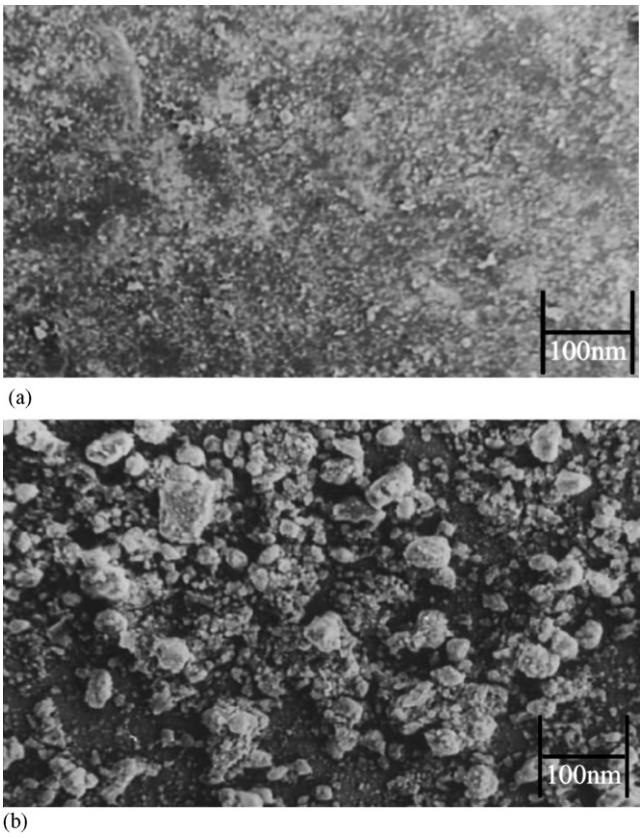

Fig. 8. SEM micrographs depicting the microstructure of ZrO_2/HAP reinforced coating on surgical grade 316L SS.

found with extensive cracking, with the resulting "Craze" (random) patterns indicative of an isotropic biaxial tensile stress state in the coating [18]. This observation is consistent with full in plane relief of shrinkage (capillary) stresses during sol–gel film drying and annealing as expected for the case of a film that is not rigidly attached to the underlying substrate. Implied in this situation is a relatively higher final film thickness compared to a well adhering film because shrinkage is not strictly confined to the thickness.

The effects of the additions of zirconia on the mechanical properties of HAP/YSZ coatings such as shear strength is given in Table 3. HAP coatings showed the lowest bond strength, and zirconia reinforced coating shows highest bond strength. The bond strength of the reinforced coatings has been improved by the addition of zirconia.

Table 3
Shear strength of HAP/YSZ reinforced coatings

ZrO_2 content (vol.%)	Shear strength (MPa)
0	17.36 ± 1.48
10	22.47 ± 2.31
30	27.32 ± 1.73
50	32.15 ± 2.54

3.2. Osteoblasts adhesion and proliferation on reinforced ceramic coatings

Fig. 10 shows the light micrographs of the zirconia reinforced HAP coatings on 316L SS substrates seeded with osteoblasts. The cells adhered on the coatings after 6 h of culture, and showed round morphology (Fig. 10a). After 24 h of culture, the cells exhibited an elongated and flattened appearance (Fig. 10b). The high magnification SEM micrograph shows that osteoblasts attached on the ceramics and minor filopodia could be observed (Fig. 11). Fig. 12 shows the results of osteoblasts proliferation on the reinforced ceramics. The mean cell number increased significantly ($p < 0.05$) with the increase of culture time and reached a density of 5500 cells/cm^2 after 5 days of culture. The results showed that osteoblasts adhered and spread well on the reinforced ceramic-coated substrates. In addition, the numbers of osteoblasts adhered on the ceramics proliferated with the increase of culture time, indicating good in vitro biocompatibility of the reinforced ceramic coatings.

3.3. In vitro electrochemical studies

3.3.1. OCP–time measurement

The OCP–time plots for the pristine, HAP and various composition of zirconia reinforcement with HAP dip coated on

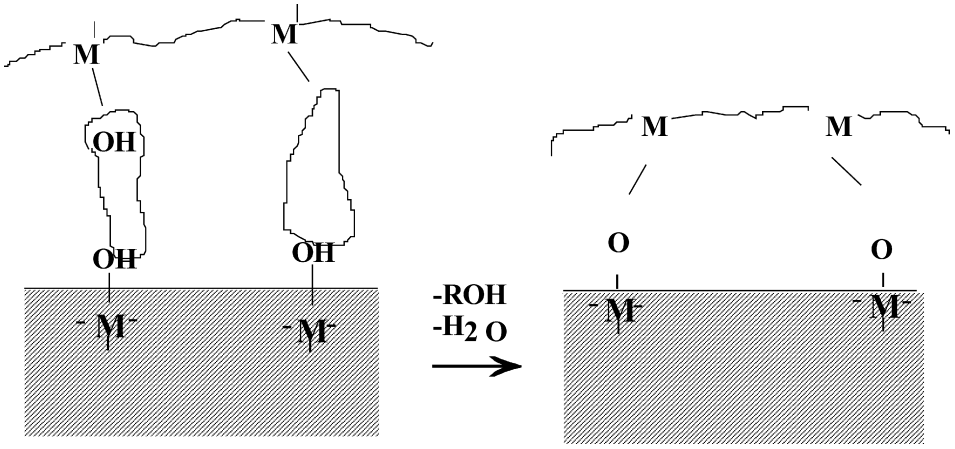

Fig. 9. A proposed adhesion mechanism for sol–gel oxide films on metal substrates showing condensation reactions between alkoxide molecules and free hydroxyl groups associated with the passivated oxide layer.

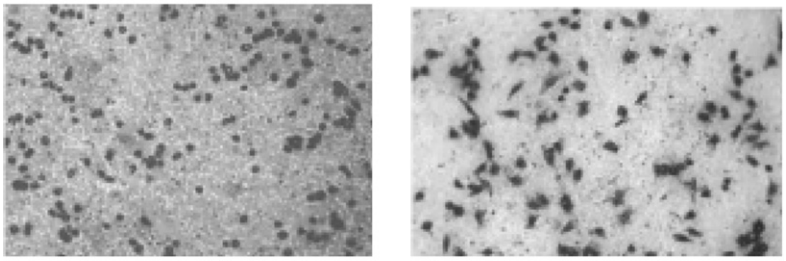

Fig. 10. Light micrographs of zirconia reinforced HAP coatings seeded with osteoblasts and cultured for different time periods: (a) 6 h, (b) 24 h.

316L SS with varied coating thickness in Ringer's solution are shown in Fig. 13. A noble shift was observed for all the coatings, with reinforcements showing better behavior than the OCP value of individual HAP coating. The OCP was found to increase with an increase in zirconia concentration and a maximum shift was observed for HAPZ3O reinforcement coating with a coating thickness of 20 μm. The enhanced values of the OCP and the attainment of stable potential can be attributed to the bifunctional nature of HAP and zirconia coatings on the metal surface.

3.3.2. Cyclic polarization studies

The cyclic polarization data were obtained for HAP with various combination of zirconia reinforced HAP (HAP + Z10, HAP + Z30 and HAP + Z50) on comparison with pristine 316L SS in Ringers solution. The E_b and E_p values for all the coated samples (625, 765 and 735 mV) are in positive direction. The HAP + Z30 reinforcement coating showed better performance among the three reinforcements. Hence, HAP + Z30 was taken for the detailed study. Table 4 shows the polarization data for HAP + Z30 with varied coating thickness. The breakdown potential for samples coated with a thickness of 20 μm was found to be around +765 mV. The breakdown potential of all the coated samples were found to be nobler than uncoated 316L SS. The kinetic parameters E_b and E_p for pristine 316L SS were +320, −35 mV, respectively, the breakdown potential and repassivation potential of HAP individual coating remains at +568 and +60 mV. It means that HAP and reinforced coatings are more corrosion resistant than uncoated 316L SS. Therefore, reinforced HAP coating on metallic substrate caused significant changes on the corrosion behavior of the metal substrate.

The individual coating of HAP could increase the E_b value of 316L SS substrate in physiological solutions but this effect was not adequately complete due to the structure and surface morphology of individual HAP coating. In the case of zirconia reinforcements, the coatings act as a barrier for the metal ion release from the metallic substrates. This is attributed to the substantial role on the formation of strong intact pore free nature of the ZrO_2/HAP coating. No detachment of the coated surface was observed after polarization. The polarization results are in good agreement with the mechanical property of the zirconia reinforced coatings.

3.3.3. Impedance analysis

The R_p values were found to be increased up to the thickness of 20 μm of zirconia reinforced HAP coating on surgical grade 316L SS and then the value decreases gradually. All diagrams showed a typical spectrum of a passivated surface, i.e., almost a capacitive behavior. Significant changes in the R_p values form 3.7588×10^6 to 6.5766×10^6 Ω for zirconia reinforced HAP coated and 2.226×10^5 to 4.8078×10^5 Ω for uncoated 316L SS were observed. The capacitance (C) were obtained at their respective breakdown potentials (R_p and values of 1.0901×10^6 Ω and 5.2210×10^{-5} for reinforced HAP coated sample). This indicates that the materials are still in the passive state. The most significant feature of the impedance curves for uncoated 316L SS is that the diameter of the semicircle decreases with the increase in applied potential, thus implying

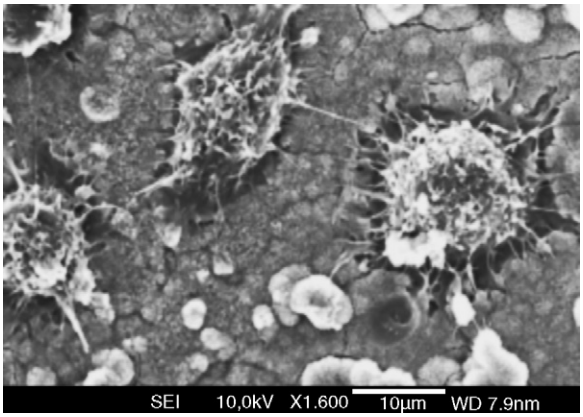

Fig. 11. SEM morphology of the reinforced HAP bioceramic coatings seeded with osteoblasts and cultured for 24 h.

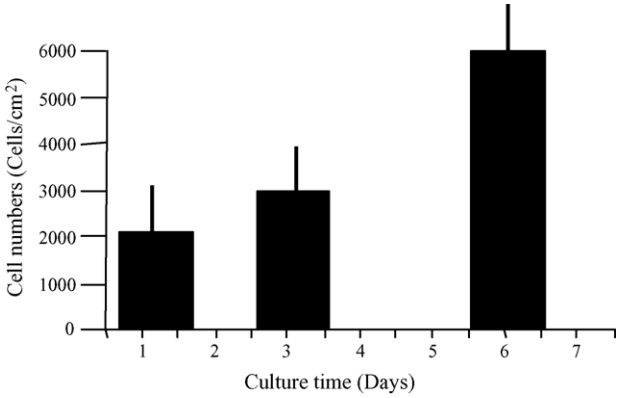

Fig. 12. Osteoblasts proliferation after 1, 3 and 5 days of culture on reinforced HAP.

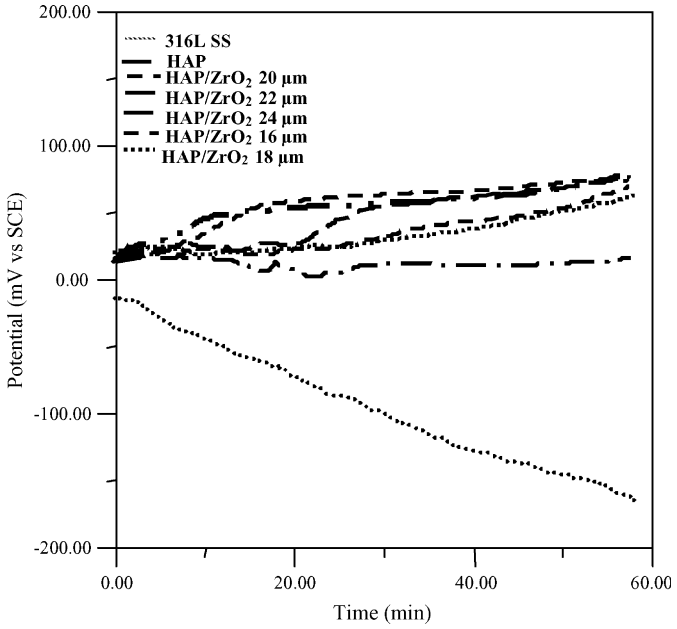

Fig. 13. OCP–time measurements in Ringer's solution of uncoated and zirconia reinforced HAP coated 316L SS obtained with varied coating thickness.

an increase in corrosion rate, which corresponds to higher dissolution within the pit [19]. This is due to the area effect resulting from enhanced degradation of the 316L SS, which is associated with high capacitance. High capacitance values were observed for pristine 316L SS whereas for the zirconia reinforced HAP coated samples only a gradual increase was observed. This could be due to the presence of coating, which prevents the pit growth. The zirconia reinforced coating shows higher polarization resistance than that of the individual coatings of HAP and zirconia. The values obtained by EIS analysis are in good agreement with the polarization data. The reinforced coating serves better than that of the individual coatings.

Table 4
Corrosion kinetic parameters for ZrO_2/HAP reinforced coatings on 316L SS

S. No.	Description	Kinetic parameter	
		E_b (mV)	E_p (mV)
1	Pristine 316L SS	+320	−35
2	HAP	+568	+60
3	ZrO_2/HAP with 16 μm thickness	+613	+214
4	ZrO_2/HAP with 18 μm thickness	+637	+240
5	ZrO_2/HAP with 20 μm thickness	+765	+389
6	ZrO_2/HAP with 22 μm thickness	+656	+248
7	ZrO_2/HAP with 24 μm thickness	+648	+227

3.3.4. Accelerated leaching study

In accelerated leaching study the concentration of the metal ions, namely Fe, Cr, Ni, Mo and the concentration of Ca, P and Zr present in the test solution are illustrated in Fig. 14. It is seen that significant amounts of metal ions were released into the solution even in the passive region for 316L SS. HAP and ZrO_2 individual coating showed little tendency for the leaching of metal ions compared to uncoated 316L SS at impressed potentials of +200, +300, +400 and E_b The release of metal ions

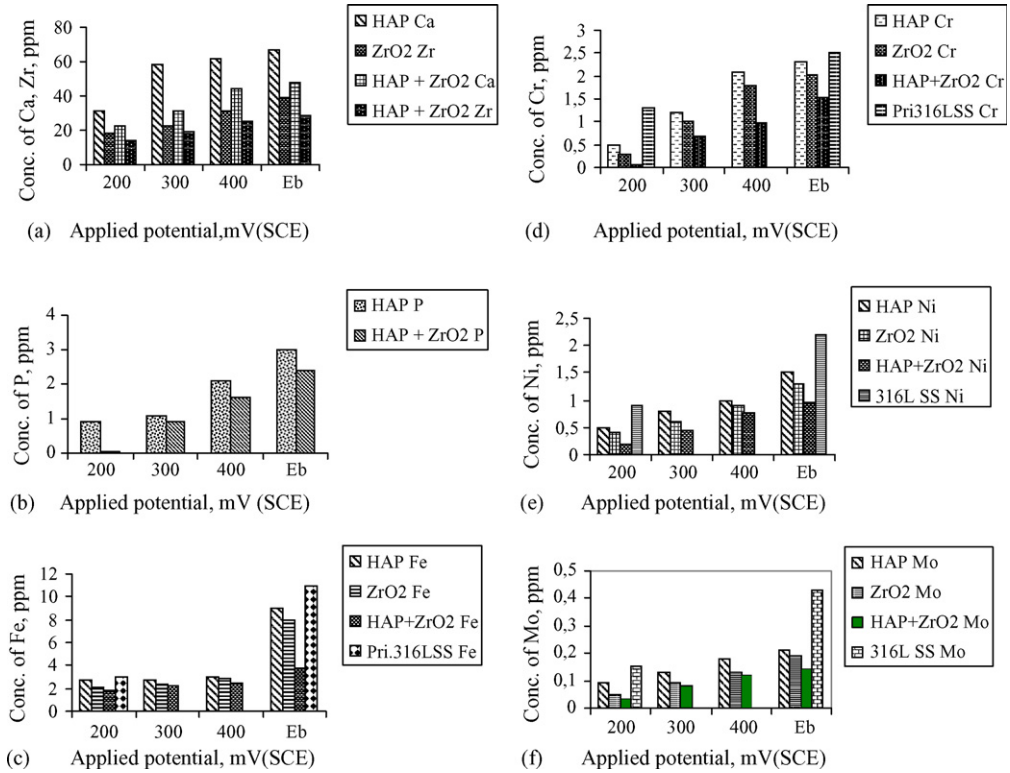

Fig. 14. Concentration of (a) calcium and zirconium (b) phosphorous (c) iron (d) chromium (e) nickel and (f) molybdenum present in Ringer's solution after accelerated leaching of pristine and zirconia reinforced HAP coated surgical grade 316L SS at various applied potentials.

from the zirconia reinforced HAP (20 μm thickness) is very low towards other coating conditions. This may be due to the grain size and distribution of the HAP and zirconia particles. The reduced leach out of metal ions and the coating elements are mainly due to the extremely regular surface topography of the coating on 316L SS. The reduced rate of the metal ion leach out is directly supported by the polarization results and impedance analysis. All the three techniques are illustrating higher stability of the zirconia reinforced HAP coating.

4. Conclusion

Several factors have taken into account when designing the bioceramics for allowing bone ingrowth. Zirconia, irrespective of its morphology and phase composition, does not alter the hydroxyapatite matrix in ZrO_2/HAP reinforced coating produced by sol–gel dip coating method. Osteoblasts adhered and spread well on the surface of the reinforced bioceramic coatings, and osteoblasts proliferation was obvious with the increase of the culture time. The results indicate that the reinforced ceramics possess good in vitro bioactivity and biocompatibility, and may be used as bioactive bone repair materials. However, further in vivo studies need to be conducted to explore the applicability of these ceramics as implant materials. Based on the structural, morphological, electrochemical and viability results, zirconia reinforced hydroxyapatite sol–gel coatings on 316L stainless steel material will serve as a potential reinforced bioceramic coating for biomedical applications.

Acknowledgement

Authors wish to acknowledge the financial support of ICMR, New Delhi, India and INSERM, ERM 0203, Uivérsity de Reims, France.

References

[1] L.L. Hench, Bioceramics: from concept to clinic, J. Am. Ceram. Soc. 74 (1991) 1487–1510.
[2] Z. LeGeros, J.P. LeGeros, G. Daculsi, R. Kijkowska, Calcium phosphate biomaterials: preparation, properties and biodegradation, Encycl. Handbook Biomater. Bioeng. 2 (1995) 1429–1463.
[3] P. Ducheyne, Q. Qiu, Bioactive ceramics: the effect of surface reactivity on bone formation and bone cell function, Biomaterials 20 (1999) 2287–2303.
[4] V.V. Silva, F.S. Lameiras, R.Z. Dominguez, Microstructural and mechanical study of zirconia-hydroxyapatite (ZH) composite ceramics for biomedical applications, Compos. Sci. Technol. 61 (2001) 301–310.
[5] L. Fu, K.A. Khor, J.P. Lim, Yttria stabilized zirconia reinforced hydroxyapatite coatings, Surf. Coatings Technol. 127 (2000) 66–75.
[6] S.L. Ishaug, M.J. Yaszemski, R. Bizios, A.G. Mikos, Osteoblast function on synthetic biodegradable polymers, J. Biomed. Mater. Res. 28 (1994) 1445–1453.
[7] R.A. Hirst, H. Yesilkaya, E. Clitheroe, A. Rutman, N. Dufty, T.J. Mitchell, C.O. Callaghan, P.W. Andrew, Sensitivities of human monocytes and epithelial cells to pneumolysin are different, Infect. Immun. 70 (2002) 1017–1022.
[8] S. Kannan, A. Balamurugan, S. Rajeswari, Electrochemical evaluation of hydroxyapatite coatings on HNO_3 passivated 316L SS for implant applications, Electrochim. Acta 50 (2005) 2065–2072.
[9] J. Li, L. Hermansson, R. Söremark, High strength biofunctional zirconia: mechanical properties and static fatigue behavior of zirconia–apatite composites, J. Mater. Sci.: Mater. Med. 4 (1993) 50–54.
[10] T. Matsuno, K. Watanabe, K. Ono, M. Koishi, Microstructure and mechanical properties of sintered body of zirconia coated hydroxyapatite particles, J. Mater. Sci. Lett. 19 (2000) 573–576.
[11] R.B. Heimann, T.A. Vu, Effect of CaO on thermal decomposition during sintering of composite hydroxyapatite–zirconia mixtures for monolithic ceramic implants, J. Mater. Sci. Lett. 16 (1997) 437–439.
[12] N. Kawashima, K. Soetanto, K. Watanabe, K. Ono, T. Matsuno, The surface characteristics of the sintered body of hydroxyapatite-zirconia composite particles, Colloids Surf. B: Biointerf. 10 (1997) 23–27.
[13] V.V. Silva, F.S. Lameiras, Z.I.P. Lobato, Biological reactivity of zirconia-hydroxyapatite composites, J. Biomed. Mater. Res. 63 (2002) 583–590.
[14] E. Adolfsson, P. Alberius-Henning, L. Hermansson, Phase analysis and thermal stability of hot isostatically pressed zirconia-hydroxyapatite composites, J. Am. Ceram. Soc. 83 (2000) 2798–2802.
[15] A. Rapacz-Kmita, A. lósarczyk, Z. Paszkiewicz, C. Paluszkiewicz, Phase stability of hydroxyapatite–zirconia (HAp–ZrO_2) composites for bone replacement, J. Mol. Struct. 704 (1–3) (2004) 333–340.
[16] A. Rapacz-Kmita, A. lósarczyk1, Z. Paszkiewicz, D. Paluch, Evaluation of HAp-ZrO_2 composites and monophase HAp bioceramics. In vitro study, J. Mater. Sci. 39 (18) (2004) 5865–5867.
[17] R. Ramachandra Rao, T.S. Kannan, Synthesis and sintering of hydroxyapatite-zirconia composites, Mater. Sci. Eng. C. 20 (1–2) (2002) 187–193.
[18] Z.J. Shen, E. Adolfsson, M. Nygren, L. Gao, H. Kawaoka, K. Niihara, Dense hydroxyapatite-zirconia ceramic composites with high strength for biological applications, Adv. Mater. 13 (3) (2001) 214–216.
[19] S. Kannan, A. Balamurugan, S. Rajeswari, Electrochemical evaluation of hydroxyapatite coatings on HNO_3 passivated 316L SS for implant applications, Electr. Acta 50 (2005) 2065–2072.